Analytical Static Stress Analysis of First Cervical Vertebra (Atlas)

E C Teo,*BSc, MSc, PhD, H W Ng,**BEng

Abstract

Introduction: *Fracture of the atlas was first described by Jefferson (1920). He theorised a bursting mechanism of fracture as the occipital condyles were driven into the atlas. Experimental studies by Hays and Alker (1988) and Panjabi et al (1991) were also conducted to explain the injury mechanisms. Injury mechanisms and fracture patterns are important in the clinical evaluation of spinal injuries. Recognition and interpretation of the fracture patterns help to determine the spinal instability and consequently the choice of treatment. Although the fracture mechanics of the atlas have received much attention, it has not been investigated using theoretical modelling.* ***Materials and Methods:*** *A high-definition digitiser was used to obtain the geometrical data for the finite element mesh generation. Contrary to the widely used method, such as computed tomography scan for geometric extraction, the direct digitising process of the dried specimen reliably preserves the accurate topography of up to 0.1-mm interval of the original structure. The finite element model was exercised under an axial compressive mode of pressure loading to investigate the sites of failure reported* **in vivo** *and* **in vitro.** ***Results:*** *Using material properties from literature, the predicted results from the 7808-finite element model demonstrate high concentration of localised stress at the anterior and posterior arch of the atlas, which agrees well with those reported in the literature. Furthermore, our results are also in good agreement with the findings reported by Panjabi et al (1991), which show that the groove of the posterior arch is subjected to enormous bending moment under simulated hyperextension conditions.* ***Conclusions:*** *The close agreement of the failure location provided confidence to perform further analysis and* **in vitro** *experiments. The predicted results from finite element analysis may be potentially used to supplement experimental research in understanding the clinical biomechanics of the C1.*

***Ann Acad Med Singapore* 2000; 29:503-9**

Key words: Atlantooccipital, Burst fracture, Cadaver

Introduction

Fractures of the atlas comprise approximately 25% of all injuries to the atlanto-axial complex, 10% of all injuries of the cervical spine, and about 2% of all spinal injuries.[1] Four-part burst fractures of the atlas were first described by Jefferson[2] in 1920. He theorised a bursting mechanism of fracture as the occipital condyles were driven into the atlas. The wedge shape of the articular pillars resulted in transmitting the axial compressive forces laterally, producing the expansile or tensile fracture at the weak points to yield one or more breaks in the bony ring. Hays and Alker[3] disputed that it was impossible to have only "one" fracture, but at least two fractures, to break the continuity of the non-elastic ring. The majority of their studies produced two-part fractures. Additional injury mechanisms would result in the so-called burst fracture of Jefferson.[1-6] To resolve the injury mechanism, many experimental studies were conducted in an attempt to determine and explain the injury mechanisms to the atlas vertebrae;[3-6] however, it has not been investigated using theoretical modelling.

One of the major limitations of any experimental study lies in its inability to quantify internal biomechanical variables such as stress distribution in the atlas. Mathematical techniques, such as a finite element model, have the potential to quantify and qualify these parameters.[7] Furthermore, the finite element model can be used to conduct parametric studies to evaluate the effect of one or more variables on the biomechanical response of the structure under non-destructive and controlled situations. This approach has been successfully used in the understanding of human lumbar and lower cervical spine.[7-12] Initial developmental efforts of spinal research using finite element methods, which started in 1970s, combined with recent advancements in the experimental area, have contributed to the success of the present-day sophisticated biomechanical analysis of the human spine.[7-11] To the best of our knowledge, a detailed finite element model of the human atlas that is geometrically accurate, however, does not exist. This finite element model was analysed preliminarily in attempting to understand the fracture mechanism of the atlas.

* *Associate Professor*
** *Research Scholar*
School of Mechanical and Production Engineering
Nanyang Technological University
Address for Reprints: Dr E C Teo, School of Mechanical and Production Engineering, Nanyang Technological University, Nanyang Ave, Singapore 639798.
E-mail: mecteo@ntu.edu.sg

In this study, a detailed three-dimensional finite element model of the cadaveric atlas was constructed with the geometrical data obtained from a three-dimensional digitiser. Using material properties from literature,[7-12] the 7808-finite element model was analysed under an axial compressive mode of pressure loading applied to its superior articular facets to predict the region of high stress concentration and comparing them with the sites of failure reported *in vivo* and *in vitro* including the fracture patterns created.

Materials and Method

The detailed, geometrically accurate three-dimensional finite element model of the atlas was developed from geometrical coordinates of a cadaveric atlas vertebra obtained using a three-dimensional digitiser (FaroArm, Bronze Series, Faro Technologies Inc, Florida, USA). The dried cadaveric atlas was obtained from a 68-year-old, male Chinese who died of old age. The cadaver was 160 cm in height and 570 N in weight. Detailed examination by independent spine surgeons found the cadaveric atlas to be within normal limits and the specimen did not show gross physical abnormalities.

As the atlas was assumed to be approximately symmetrical about the mid-sagittal plane, only half of the atlas was modelled.[1-7] A small hole was drilled into one side of the atlas, and a screw was passed through and secured by two nuts. The screw was in turn clamped in a vice-clamp. The digitiser was used to digitise the whole surface area of the half-vertebra at 0.1-mm intervals by moving the point probe over the various surface profile of the atlas. The coordinates data (about 50,000 points) obtained were stored in a microcomputer.

Calibration and setting of the reference point to define the origin of the coordinate axis set were undertaken before any measurement. The global XYZ coordinate system was set with the Y-axis acting along the mid-sagittal plane of the atlas, and the X-axis and Z-axis pointing toward the posterior and left lateral directions, respectively.

Using the computer software, Surfacer 7.0 (Structural Dynamics Research Corporation, Ohio, USA), the three-dimensional coordinate data were processed to obtain the sequential cross-section outline of the vertebra at 1- to 2-mm intervals, depending on the complexity of the geometry. It was serrated and had numerous line segments. Splines were fitted to the identified boundary points to obtain a smoother "wire frame" for each section. These three-dimensional geometrical boundary data files were converted into a universal graphics data format (IGES), which were then imported into a commercially available finite element modelling software, ANSYS (ANSYS Inc, Pennsylvania, USA) for the three-dimensional finite element mesh reconstruction. The solid model was developed in two stages: surface creation and solid definition. By defining a series of four closed-loop boundary curves from two neighbouring cross-section outlines using the line segments, a series of surfaces were created. The surfaces of the entire model were carefully re-examined against the physical model for accuracy. A solid was then generated by the creation of volume defined by its enclosing six surfaces. The solid model for the entire structure was thus developed following this procedure.

The finite element mesh was obtained by discretising the solid model using a mapped mesh technique. The mapped mesh method in ANSYS allows for the automatic creation of finite elements, which conform exactly to the shape of the defined volume. At this stage, the number of elements, element type and element size were chosen depending on the complexity of the geometry, desired problem size and analysis nature of the finite element model.

In this study, eight-noded isoparametric solid elements, instead of tetrahedron solid elements, were chosen to model the vertebra. This type of element should yield better element behaviour in the analysis.[13] The vertebra was assumed of cortical bone throughout and the internal cancellous structure was ignored. The full finite element model shown in Figure 1, symmetric at approximately the mid-sagittal plane, consisted of 7808 elements representing various spinal structures such as anterior/posterior tubercules, superior/inferior articular processes, transverse process and posterior arch of the atlas.

To exercise the finite element model, appropriate material properties for these elements were chosen. Because of lack of material definition for the atlas, values used in other regions of the vertebral column were adopted as a first step. Linear isotropic and homogenous mechanical properties using Young's modulus of 10,000 MPa and Poisson's ratio of 0.29 were assumed for the atlas.[9,10]

To simulate the experimental setups carried out by Hays and Alker[3] and Panjabi et al[5] as closely as possible, three boundary conditions were applied: Case 1—the inferior facet was fully constrained in all directions of movement; Case 2—the inferior facet was constrained to move in the supero-inferior direction; and Case 3—in addition to the conditions defined in Case 2, all the nodes on the posterior arch in the plane of symmetry restrained from moving in the antero-posterior direction. For all cases, all nodes on the anterior arch lying in the plane of symmetry were constrained in the antero-posterior direction to mimic the restrained provided by the dens of C2 and the transverse ligament. Additional analysis run under extension for Case 2 was performed to simulate the atlas hitting the axis below by applying a vertical point displacement of 0.01-mm at the posterior arch.

In order to examine how various loading configuration under different boundary conditions might alter the mechanics effect of the atlas, the model was axially loaded under three simulated head postures: 1) neutral, 2) flexion and 3) extension. A compressive force of 25N (about the weight of the head) was applied to the superior facet surface. The superior facet surface was divided into three regions: an anterior region, a middle region and a posterior region, with an approximated superior facet surface area of 150-mm^2 for pressure loading. With an area ratio of 1:2:1, for the neutral condition, a uniform pressure loading of 0.167 MPa was applied across the superior facet surface. Under flexion, an increased pressure was shifted towards the anterior region. Under extension, an increased pressure was shifted towards the posterior region as shown in Figure 2. Table I lists the distribution of pressure applied to the superior facet of the atlas under three different simulated head postures investigated in the present study.

Results

The predictions of von Mises stress distribution for loading configurations illustrated in Table I under different boundary conditions are presented in this section. Loading of 25 N is kept constant throughout the analysis. Figure 3 shows the predicted location for high concentration of localised von Mises stress. For neutral loading configurations, under different boundary conditions, the stress contours are shown in Figures 4 to 7. Figures 8 to 11 show the variation of average von Mises stress at the predicted likely failure sites under different loading configurations and boundary conditions. Finally, Figure 12 shows the predicted location and their corresponding maximum von Mises stress.

Figure 4 shows that high concentration of localised von Mises stress can be seen at the anterior arch and junction between the posterior arch and lateral mass. It can also be seen that maximum von Mises stress of 1.039 MPa occurs at the anterior arch. Figures 5 and 6 show that high concentration of localised von Mises stress is found at the anterior arch, junction between the posterior arch and lateral mass and groove of the posterior arch. In addition, Figure 5 shows that maximum von Mises stress of 1.965 MPa occurs at the inferior junction between the posterior arch and lateral mass. Furthermore, it also shows that the tip of the posterior arch moved anteriorly towards the anterior arch as the lateral mass is displaced laterally, creating tension around the outer side of the posterior arch and compression at the inner side of the posterior arch. This result differs from Figure 6, which shows that the inner side around the groove of the posterior arch is in tension due to the additional constraint provided at the tip of posterior arch (Case 3).

Figure 7 shows that the posterior arch is displaced in the anterior and superior directions creating tension at the inferior, outer side of the posterior arch and compression at the superior, inner side, producing a bending moment effect at the groove of the posterior arch. In addition, high-localised von Mises stress is seen at the inner side at the groove of the posterior arch. Figures 8 to 10 show that the average von Mises stress is higher under flexion at the anterior arch and lower at the junction of posterior arch and lateral mass. In contrast, von Mises stress is lower under extension at the anterior arch and higher at the junction junction of posterior arch and lateral mass under extension. In addition, it shows that von Mises stress at the groove of the posterior arch remains within 2% to 4% difference under different loading configurations and boundary conditions.

Furthermore, it clearly shows that von Mises stress at the anterior arch increases as the loading configurations are change from extension to neutral and finally to flexion loading configurations. For Case 2 shown in Figure 9, it is interesting to see that von Mises stress at the anterior arch increased by 60% from extension to flexion positions while the von Mises stress at the posterior arch only decreased by 20%.

Additional stress analysis of C1, by applying a vertical point displacement of 0.01mm at the tip of the posterior arch, shows that the average von Mises stress (Fig. 11) at the posterior side of the C1 increases tremendously from anterior arch to the junction of the posterior arch and lateral mass or groove of the posterior arch. The results obtained are different from the analysis for Case 2 where the average von Mises stress under extension loading increased by 70% from the anterior arch to the junction while decreasing by about 60% from the junction to the groove. The average von Mises stress from the junction to the groove of the posterior arch only shows a slight increase for Case 2 with a vertical point displacement at the tip of the posterior arch. The results also show substantial increase of average von Mises stress at the groove of the posterior arch from Case 2 to Case 2 with additional displacement, while difference in average von Mises stress at the anterior and junction of the posterior arch and lateral masses remains negligible. These results imply that the posterior arch is subjected to higher level of stress concentration when C1 hits C2.

Figure 12 summarises the predicted maximum von Mises stress and their respective locations under different loading configurations for the three cases. The results for Case 1 and Case 3 show an increase of maximum von Mises stress from neutral, flexion and finally to extended position. In summary, maximum von Mises stress increased by 45% to 51% under different loading conditions. However, for Case 2, the results show that maximum von Mises stress is highest under flexion, followed by neutral and extension loading configurations.

Fig. 1. Iso-posterior view of the finite element model.

Fig. 2. Loading configurations under extended condition.

Fig. 3. Location of localised high von Mises stress.

Fig. 4. Von Mises stress contour and undeformed edge display for neutral loading configuration under fully constraint condition at the inferior facet (Case 1). Arrows indicating the force vector of principal stresses.

Fig. 5. Von Mises stress contour and undeformed edge display for neutral loading configuration under constraint in supero/inferior directions at the inferior facet (Case 2). Arrows indicating the force vector of principal stresses.

Fig. 6. Von Mises stress contour and undeformed edge display for neutral loading configuration under constraint in supero/inferior directions at the inferior facet and all the nodes on the posterior arch in the plane of symmetry restrained from moving in the antero-posterior direction (Case 3). Arrows indicating the force vector of principal stresses.

Fig. 7. Von Mises stress contour and undeformed edge display for extended loading configuration under constraint in supero/inferior directions at the inferior facet (Case 2) and applying a vertical point displacement of 0.01 mm at the posterior arch to simulate C1 hitting C2. Arrows indicating the force vector of principal stresses.

Fig. 13. Illustration on the weak cross-section of the anterior and posterior arch. A) Anterior arch, B) groove of the posterior arch.

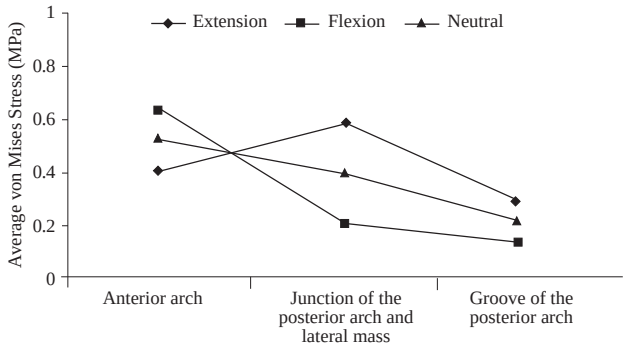

Fig. 8. Average von Mises stress under fully constraint condition at the inferior facet (Case 1).

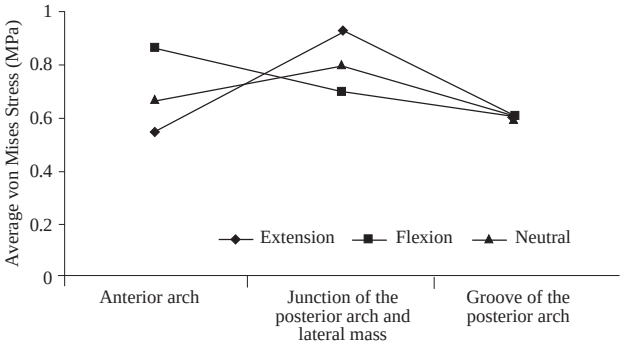

Fig. 9. Average von Mises stress under constraint in supero/inferior directions at the inferior facet (Case 2).

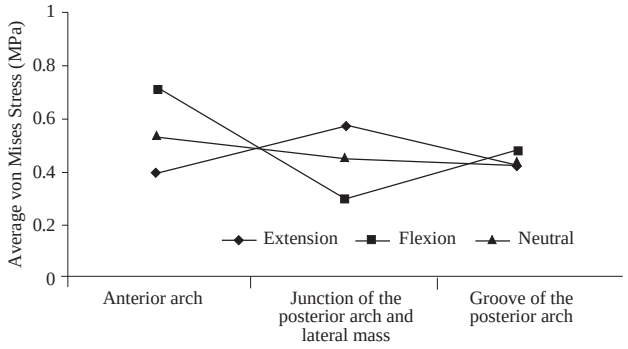

Fig. 10. Average von Mises stress under constraint in supero/inferior directions at the inferior facet and all the nodes on the posterior arch in the plane of symmetry restrained from moving in the antero-posterior direction (Case 3).

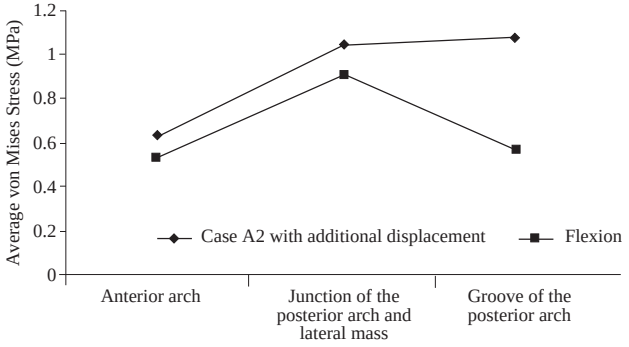

Fig. 11. Average von Mises stress under constraint in supero/inferior directions at the inferior facet (Case 2) and including an addition vertical displacement of 0.01mm applied at the tip of the posterior arch under extended loading conditions.

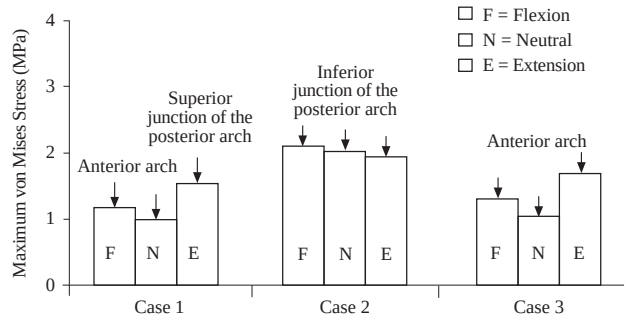

Fig. 12. Predicted location and corresponding maximum von Mises stress under different loading configurations for the three cases.

Furthermore, it is interesting to see that the different loading configurations used in the analysis do not affect the location of the maximum von Mises stress. Generally, it should be pointed out that a variation of only 8% is obtained for maximum von Mises stress under different simulated head postures for Case 2.

Discussion

The primary objective of this study was to develop a detailed three-dimensional finite element (FE) model of the human atlas using actual data from a dry specimen. All the important anatomic features of the atlas such as the facet articulation surfaces and posterior arch were clearly defined in our model. The direct digitising process of the dry specimen reliably preserves the accurate topography of the original structure that is to be replicated. Although our model may be realistic enough to produce a qualitative assessment of the likely sites of fractures, it is still very simplistic and should be applied with care to quantitative analyses. The study was also designed to determine the influence of the simulated head postures and boundary conditions that replicate the experimental setups[3,5] on the likely sites of atlas fracture under axial compressive loading. The model was analysed in flexion, neutral and extension loading configurations to simulate the different head postures as described in Table I. Table II illustrates the likely failure sites under three different loading configurations for the three boundary conditions from the FE analysis.

In the present study, the predicted likely failure sites agreed closely with the experimental results.[3,5] As expected, high concentration of localised stress can be seen at the anterior arch, junction between the posterior arch and lateral mass and groove of the posterior arch. In addition, it is clear that the experimental measurements by Hays and

Alker[3] correspond well with the present FE analysis for Case 1, which shows that the predicted location of fracture within the posterior arch did not routinely occur at the thinnest measured point of the arch (groove of the posterior arch in FE model). These results also indicated that the atlas might fracture in two or more locations in order to break the continuity of the non-elastic ring as stated by Hays and Alker.[3]

Although we used three different pretrauma head postures, namely flexion, neutral and extension loading conditions for Case 2, there was no apparent differences in the predicted von Mises stress distribution (Fig. 5). This result agrees with the observations by Panjabi et al[5] whose experiments in two different pretrauma postures did not result in different fracture pattern.

These results suggest that in reality, the fracture location of the atlas is dependent on other factors such as the force vector applied to the head, precise posture at the time of trauma, spinal geometry and physical properties, resulting in a variety of fracture patterns.

It should be pointed out that the posterior arch might be fractured by a completely different mechanism, i.e., due to hyperextension of the cervical spine (Fig. 7). Figure 13 illustrates the weakest cross-sections, and their typical cross-sectional shapes of the anterior and posterior arch. From simple engineering considerations, it shows that cross-section A is weakest when the arch is bent in the horizontal plane (about Y-axis), whereas cross-section B is weakest when the arch is bent in the sagittal plane (about Z-axis). Thus hyperextension of the cervical spine, where the posterior arches of C1 and C2 hit each other, may produce enough bending moment at the weakest cross-section of the posterior arch to produce its failure.[5] These explanations are in good agreement with our results (Fig. 7) which show that the groove of the posterior arch is subjected to high level of tensile forces at the outer, inferior side and compressive force at the inner, superior side of groove of the posterior arch, creating an enormous amount of bending moment at its weakest section to fracture the atlas.

Most previous reports on C1 fractures have been clinical in nature, but some have discussed the forces involved in burst fractures. In his original reports, Jefferson proposed that the mechanism for C1 burst fractures was the conversion of compressive forces into the expansive or horizontal forces because of the wedge-shaped cross-section of the C1 lateral masses. Since then, others have classified C1 fractures into as many as six different types and have proposed various mechanisms and treatments for each type.[14-18] Hays and Alker[3] studied the *in vitro* production of C1 burst fractures and the patterns created, but their testing method did not allow for accurate measurements of the forces involved. Panjabi et al[5] were the first to use an accurately measurable force to produce C1 burst fractures. Using occipito-cervical segments, they were able to produce fractures with forces as low as 1900 N under extended postures, but in six specimens under neutral postures with forces as high as 3100 N. These findings also correlate with our results which clearly demonstrate that von Mises stress at the likely sites of failure, under a constant loading of 25 N, increased by 35% for Case 2 (Fig. 9) from neutral to extension. The results imply that the head should not be positioned in the extended posture if large axial loads are applied to the head.

Although C1 fractures do not occur in isolation from the surrounding bones and soft tissues, the analysis method used in the current study eliminated variability in the load application and in the fracture patterns of the C1 ring. The authors examined the response to applied axial force alone, which is the force vector believed to produce these fractures *in vivo*.

It has been pointed out that a mathematical model based on high quality experimentally obtained, physical data is likely to represent the real structure successfully with a limited validation.[19] Two of the most important physical

TABLE I: THE THREE CONFIGURATIONS EXPLORED

Configuration	Description	Superior facet surface pressure (MPa)		
		Anterior	Middle	Posterior
1	Neutral	0.167	0.167	0.167
2	Flexion	0.267	0.167	0.067
3	Extension	0.067	0.167	0.267

TABLE II: PREDICTED FAILURE SITES USING FINITE ELEMENT METHODS

Case	Failure possibility								
	Anterior arch			Junction between posterior arch and lateral mass			Groove of the posterior arch		
	Flexion	Neutral	Extension	Flexion	Neutral	Extension	Flexion	Neutral	Extension
1	High	High	Low	High	High	High	Low	Low	Low
2	High	High	Moderate	High	High	High	High	High	High
3	High	High	Low	High	High	High	Moderate	Moderate	Moderate

data in constructing a FE model of the atlas are geometric and material properties. For the FE model to be effective, it is desirable for an FE model of the atlas to process high-quality representations of these aspects. It has been shown that bony geometry of the cervical spine greatly affects its biomechanical responses.[20] Although our model is very realistic, the current results are limited by the use of linear elastic and homogeneous material properties. It is well known that human cervical response is nonlinear. These assumptions reduce the complexity of the analysis but do not replicate the nonlinear postyield behaviour of the vertebral body's trabecular bone. Nevertheless, loads were applied consistent with physiologic loading conditions in which overt failure is not expected to occur. Despite this, the results may potentially be extrapolated to investigate failure behaviour of C1 as linear models have been successfully used to predict fractures of the pedicle and proximal femur.[12,21]

Another limitation of the present study is the use of static analysis procedures. To simulate traumatic loading situations as in experimental loadings carried out by Panjabi et al,[5] it may be prudent to incorporate appropriate dynamics-related variables and exercise the FE model under high-speed loading. A logical extension of the existing FE model would be to include additional levels so that the C1-C2-C3 mechanics can be delineated. We are advancing our studies to include these features.

Other limitations of the present model are the boundary conditions. In reality, the atlas is not constrained from moving in space, however, that was the boundary constraint assigned to the inferior articular facet surface of the atlas in the present FE analysis.

Conclusions

In summary, a three-dimensional geometrical and mechanical accurate finite element model based on actual geometry has been successfully developed for C1. To the best of our knowledge, no studies are currently available that incorporated the complex geometry of the C1 in a detailed finite element model. The model was validated against experimental data[3,5] under the axial compressive mode of loading based on the material properties from literature. The close agreement of the failure location provided confidence to perform further analysis and *in vitro* experiments.

The results show that finite element method is an invaluable application that can supplement experimental research in understanding the clinical biomechanics of the C1. This method may also guide us in developing better experimental designs. Furthermore, because of its reproducibility and repeatability, a fully validated model can be used to analyse detailed parametric studies of novel instrumentations, allowing for the avoidance of otherwise costly experimentation. In addition, the results will provide further understanding of injury mechanisms of the atlas, which is important for the prevention, diagnosis and treatment of spinal injuries.

REFERENCES

1. Levine A M, Edwards C C. Treatment of injuries in the C1-C2 complex. Orthop Clin North Am 1986; 17:31-44.
2. Jefferson G. Fracture of the atlas vertebra: Reports of four cases and a review of those previously recorded. Br J Surg 1920; 7:407-22.
3. Hays M B, Alker G J. Fracture of the atlas vertebra: The two-part burst fracture of jefferson. Spine 1988; 13(Pt6):601-3.
4. Mouradian W H, Fietti Jr V G, Cochran G V B, Fielding J W, Young J. Fractures of the odontoid: A laboratory and clinical study of mechanisms. Orthop Clin North Am 1978; 9:985-1001.
5. Panjabi M M, Oda T, Crisco J J, Oxland T R, Katz L, Nolte L. Experimental study of atlas injuries I: Biomechanical analysis of their mechanicsms and fracture patterns. Spine 1991; 16:S460-S465.
6. Oda T, Panjabi M M, Crisco J J, Oxland T R, Katz L, Nolte L. Experimental study of atlas injuries II: Relevance to clinical diagnosis and treatment. Spine 1991; 16:S466-S473.
7. Maiman D J, Sances A, Myklebust J B. Compression injuries of the cervical spine: A biomechanical analysis. Neurosurgery 1983; 13:254-60.
8. Gilbertson L G, Goel V K, Kong W Z, Clausen J D. Finite element methods in spine biomechanics research. Crit Rev Biomed Eng 1995; 23(Pt5&6):411-73.
9. Yoganandan N, Myklebust J B, Ray G, Sances A. Mathematical and finite element analysis of spine injuries. Crit Rev Biomed Eng 1987; 15(Pt1):29-89.
10. Yoganandan N, Kumaresan S, Voo L, Pintar F A. Finite element applications in human cervical spine modeling. Spine 1996; 21(Pt15): 1824-34.
11. Yoganandan N, Kumaresan S, Voo L, Pintar F A. Finite element model of the human lower cervical spine: parametric analysis of the c4-c6 unit. J Biomech Eng 1997; 119(Pt3):87-92.
12. Whyne C M, Hu S S, Klisch S, Lotz J C. Effect of the pedicle and posterior arch on vertebral body strength predictions in finite element modeling. Spine 1998; 23(Pt8):899-907.
13. Kardestuncer H. Finite Element Handbook. New York: McGraw-Hill, 1987.
14. Landells C D, Peteghem P K V. Fractures of the atlas: Classification treatment and morbidity. Spine 1988; 13(Pt5):450-2.
15. Lee T T, Green B A, Petrin D R. Treatment of stable burst fracture of the atlas (Jefferson fracture) with rigid cervical collar. Spine 1998; 23(Pt18):1963-7.
16. Kesterson L, Benzel E, Orrison W, Coleman J. Evaluation and treatment of atlas burst fractures (Jefferson fractures). J Neurosurg 1991; 75:213-20.
17. Segal L S, Grimm J O, Stauffer E S. Non-union of fractures of the atlas. J Bone Joint Surg 1987; 69(Pt9):1423-34.
18. Levine A M, Edwards C C. Fractures of the atlas. J Bone Joint Surg 1991; 73(Pt5):680-91.
19. Panjabi M M. Validation of mathematical models. J Biomech 1979; 12:238.
20. Yoganandan N, Pintar F A, Sances A, Reinsartz J, Larson S J. Strength and motion analysis of the human head-neck complex. J Spinal Disord 1991; 4:73-85.
21. Lotz J P, Cheal E J, Hayes W C. Fracture prediction for the proximal femur using finite element models: Part I-linear analysis. J Biomech Eng 1991; 113:353-60.